Composites: Part B 41 (2010) 106–115

Contents lists available at ScienceDirect

Composites: Part B

journal homepage: www.elsevier.com/locate/compositesb

Characterizing elastic properties of carbon nanotubes/polyimide nanocomposites using multi-scale simulation

Jia-Lin Tsai [a,*], Shi-Hua Tzeng [a], Yu-Tsung Chiu [b]

[a] Department of Mechanical Engineering, National Chiao Tung University, Hsinchu 300, Taiwan
[b] Materials Research Lab., Industrial Technology Research Institute, Hsinchu 310, Taiwan

ARTICLE INFO

Article history:
Received 18 December 2008
Accepted 7 June 2009
Available online 18 June 2009

Keywords:
A. Nano-structures
C. Micro-mechanics
B. Mechanical properties
Molecular dynamics

ABSTRACT

This research is aimed at characterizing the elastic properties of carbon nanotubes (CNTs) reinforced polyimide nanocomposites using a multi-scale simulation approach. The hollow cylindrical molecular structures of CNTs were modeled as a transverse isotropic solid, the equivalent elastic properties of which were determined from the molecular mechanics calculations in conjunction with the energy equivalent concept. Subsequently, the molecular structures of the CNTs/polyimide nanocomposites were established through molecular dynamics (MD) simulation, from which the non-bonded gap as well as the non-bonded energy between the CNTs and the surrounding polyimide were evaluated. It was postulated that the normalized non-bonded energy (non-bonded energy divided by surface area of the CNTs) is correlated with the extent of the interfacial interaction. Afterwards, an effective interphase was introduced between the CNTs and polyimide polymer to characterize the degree of non-bonded interaction. The dimension of the interphase was assumed equal to the non-bonded gap, and the corresponding elastic stiffness was calculated from the normalized non-bonded energy. The elastic properties of the CNT nanocomposites were predicted by a three-phase micromechanical model in which the equivalent solid cylinder of CNTs, polyimide matrix, and the effective interphase were included. Results indicated that the longitudinal moduli of the nanocomposites obtained based on the three-phase model were in good agreement with those calculated from MD simulation. Moreover, they fit well with the conventional rule of mixture predictions. On the other hand, in the transverse direction, the three-phase model is superior to the conventional micromechanical model since it is capable of predicting the dependence of transverse modulus on the radii of nanotubes.

1. Introduction

Because of their exceptional mechanical properties, carbon nanotubes (CNTs) have been extensively utilized as reinforcements in composite materials [1,2]. Because the dimensions of the CNTs are within nanoscale while the polymer itself is often regarded as a bulk matrix material in composites, it becomes a challenging issue to properly characterize the properties of the CNT/polymer hybrids using the conventional continuum theory. In the past decade, the mechanical properties of CNT-reinforced nanocomposites have been modeled by many researchers using the molecular dynamics (MD) simulation [3–5], continuum mechanics [6–8], and multi-scale simulation [9,10].

Han and Elliott [3] investigated the mechanical properties of nanocomposites with various volume fractions of single-walled (10,10) CNTs embedded in amorphous polymer matrix. Results indicate that when the interaction between the CNTs and polymer is strong, the interfacial effect cannot be ignored in the material modeling. The elastic moduli for the single-walled CNTs/polyethylene nanocomposites were predicted by Griebel and Hamaekers [4] using MD simulation. For the nanocomposites with very long CNTs, the longitudinal modulus demonstrated excellent agreement with the predictions by micromechanical rule of mixtures. Zhu et al. [5] performed MD simulation on single-walled CNT-reinforced Epon 862 matrix, indicating that long CNTs can greatly improve the moduli of the nanocomposites. According to the results in the literature [4,5], it seems that the atomistic interaction between the CNTs and polymer may not have a significant effect on the longitudinal modulus of a nanocomposite, if it is reinforced by the long CNTs. Moreover, the moduli of the nanocomposites can be properly modeled using the continuum micromechanics model (rule of mixture). Liu and Chen [6] proposed a representative volume element based on the continuum mechanics to evaluate the effective mechanical properties of CNT nanocomposites. Finite element results revealed that the load carrying capacities of CNTs in nanocomposites were significant. Luo et al. [7] investigated the effects of spatial distribution and geometry of CNTs on the modulus of

* Corresponding author. Tel.: +886 3 5731608; fax: +886 3 5720634.
E-mail address: jialin@mail.nctu.edu.tw (J.-L. Tsai).

1359-8368/$ - see front matter © 2009 Elsevier Ltd. All rights reserved.
doi:10.1016/j.compositesb.2009.06.003

CNT nanocomposites using finite element analysis. Results illustrated that the effects of fiber volume fraction and aspect ratio were similar to those of conventional short-fiber composites. Because the interfacial effects are not taken into account in continuum mechanics modeling, some essential characteristics in atomistic/nanoscales may be disregarded in the continuum analysis [6,7]. The comparative study of the continuum micromechanical models employed in the prediction of elastic properties of single-walled nanocomposites was provided by Selmi et al. [8]. Hammerand et al. [9] conducted micromechanical analysis on the CNT nanocomposites by introducing an interphase layer between the CNTs and the matrix to simulate the imperfect load transfer or imperfect bonding. The dimension of the interphase was determined such that the interphase has the same volume fraction as the CNTs. Gates et al. [10] provided details on the current approach to multi-scale modeling and simulation of advanced materials such as nanotube-reinforced polymer composites for structural applications. Among the aforementioned approaches, it has been found that the longitudinal properties of the CNT composites are mostly of concern whereas the investigations on the transverse properties are relatively few. In addition, the effects of atomic interaction between the CNTs and the surrounding polymer, which may play an important role in the mechanical responses of the nano-structured materials, are rarely explored and considered in the material modeling.

In this study, the simulation methodology basically has been divided into two parts. The first one is to establish an equivalent solid cylinder with proper mechanical properties, taking the place of atomistic structures of CNTs in the CNT-reinforced nanocomposites. In the second part, the extent of atomistic interaction between the CNT atoms and the surrounding polyimide polymer has been modeled by an effective interphase such that the information of the atomistic interaction, which is in atomic scale, can be taken into account in the continuum media. Eventually, the mechanical properties of CNT/polyimide nanocomposites were characterized using the continuum micromechanical model, and the results were compared with those obtained directly from the MD simulations.

2. Equivalent solid cylinder

2.1. Construction of equivalent solid cylinder

The configuration of CNTs is a hollow, cylindrical structure that consists of hexagonal carbon rings. As reinforcements in composite materials, the fundamental mechanical properties of the CNTs should be defined in the conventional manner of mechanics such that the existing micromechanical model can be directly implemented into the CNT nanocomposites [11,12]. In general, the reinforcements in the mechanics of composites are regarded as a solid with homogeneous material properties. Apparently, the original attributes of cylindrical hollow structure of CNTs cannot satisfy the stated requirement; therefore, it is necessary to have an equivalent solid cylinder so that the mechanical properties of the atomistic CNT structure can be properly interpreted in the continuum solid model and precisely transformed into the CNTs nanocomposites. It has been assumed that the equivalent solid cylinder has the same geometric configuration as those of the original CNTs structures. In other words, the radius of the equivalent solid cylinder is equal to the distance measured from the center of a CNT to the circumferential atoms, as shown in Fig. 1. In this study, only zig-zag type single-walled CNTs, i.e., (10,0), (14,0), and (18,0), with radii, 3.9, 5.5, and 7.1 Å, were selected for the demonstration, but the approach presented hereafter is not limited to these cases.

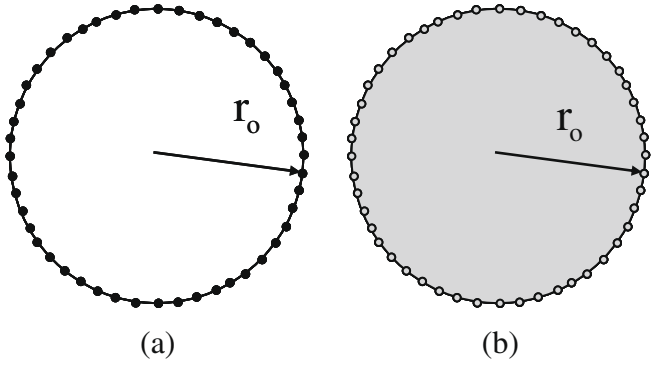

Fig. 1. Schematic diagram of single-walled CNTs cross-section: (a) atomistic CNTs structure, (b) equivalent solid cylinder.

2.2. Determination of mechanical properties of the equivalent solid cylinder

In addition to the geometric configuration, the associated mechanical properties of the equivalent solid cylinder have to be determined properly in accordance with the atomistic structures of CNTs. Because of the geometric configuration of the CNTs, the corresponding properties of the equivalent solid cylinder were assumed to be transversely isotropic. In other words, there are five independent material constants in the effective solid required to be evaluated. To accomplish this objective, the discrete atomistic structures of CNTs with energy minimization were constructed in the beginning using MD simulation. Subsequently, by applying a desired displacement on the CNTs, the strain energy variation in terms of the deformation was calculated. Meanwhile, the same deformation was applied to the equivalent solid. According to the hypothesis that the strain energy variations in the CNT atomistic structure and the equivalent solid continuum in terms of the same deformation should be the same, the corresponding material constants in the equivalent solid were evaluated.

2.2.1. Construction of CNT molecular structures

The fundamental mechanical properties of CNTs were characterized using MD simulation in which the molecular structures of CNTs as well as the atomistic interaction have to be constructed and specified appropriately. The zig-zag type CNTs with 85.2 Å in length were constructed by repeating the unit cell several times along its axial direction (1 direction) as shown in Fig. 2.

In the MD simulation, two kinds of atomistic interactions have been taken in account in the modeling of CNTs; one is bonded interaction, such as the covalent bonding, and the other one is the non-bonded interaction, i.e., van der Waals and electrostatic forces. For the CNTs, the primary structure was constructed by the bonded atomistic interaction between the carbon atoms. Such bonded interaction can be described using the potential energy that consists of bond stretching, bond angle bending, torsion, and inversion as illustrated in Fig. 3 [13]. The explicit form of the total potential energy for bonded interaction is expressed as

$$U_{\mathrm{CNT}} = \sum U_r + \sum U_\theta + \sum U_\phi + \sum U_\omega \tag{1}$$

where U_r is a bond stretching potential; U_θ is a bond angle bending potential; U_ϕ is a dihedral angle torsional potential; and U_ω is an inversion potential. For small deformations, the stretching and bending behaviors can be modeled using elastic springs and then the corresponding potentials can be approximated as [14]

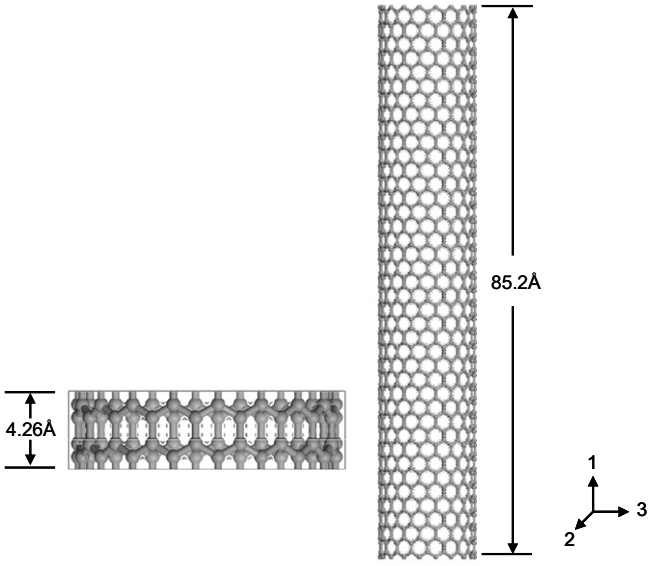

Fig. 2. Schematic depiction of a zig-zag type (18,0) CNT unit cell.

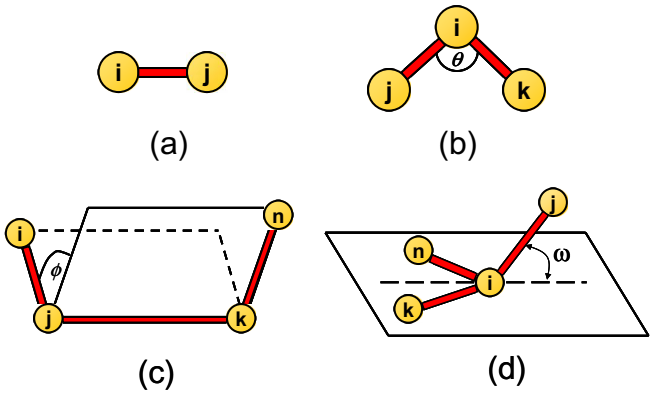

Fig. 3. A schematic representation of the inter-atomic potential: (a) bond stretch, (b) bond angle bending, (c) dihedral angle torsion, and (d) inversion.

$$U_r = \frac{1}{2}k_r(r - r_0)^2 \tag{2}$$

$$U_\theta = \frac{1}{2}k_\theta(\theta - \theta_0)^2 \tag{3}$$

For the dihedral torsional potential and inversion potential, Li and Chou [14] adopt the simplest harmonic form to incorporate the two interactions together into a single equivalent term as

$$U_\tau = U_\phi + U_\omega = \frac{1}{2}k_\tau(\phi - \phi_0)^2 \tag{4}$$

In Eqs. (2)–(4), k_r, k_θ, and k_τ are the bond stretching force constant, angle bending force constant, and torsional resistance, respectively. The constants $k_r = 93,800\,\frac{\text{kcal}}{\text{mol nm}^2}$ and $k_\theta = 126\,\frac{\text{kcal}}{\text{mol rad}^2}$ selected from AMBER force field for carbon–carbon atomic interaction [15], were employed in the present molecular simulation. On the other hand, for the force constant k_τ, since Li and Chou [14] indicated that this value may not have significant influence on CNT's Young's modulus, we directly adopted the constant $k_\tau = 40\,\frac{\text{kcal}}{\text{mol rad}^2}$ from the literature. The parameters r_0, θ_0, and ϕ_0 represent bond length, bond angle, and dihedral torsional angle in equilibrium position, which are equal to 1.42 Å, 120°, and 180°, respectively, in the CNTs atomistic structures. It should be noted that the DL-POLY package originally developed by Daresbury Laboratory [16] was employed for the current MD simulation, in which Dreiding potential [17] was utilized to model the inter-atomic potential of carbon–carbon bonding. For the bond stretching and angle changing behaviors, the mathematical forms in Dreiding potential are exactly the same as those given in Eqs. (2) and (3). Nevertheless, for the dihedral torsion and inversion, the Dreiding torsional potential that accounts for the two portions together, could be expressed as

$$U_\tau = U_\phi + U_\omega = A[1 - \cos(m(\phi - \phi_0))] \tag{5}$$

Because the carbon–carbon bonding in the hexagonal graphite is in resonance, the parameter m in Eq. (5) should be equal to 2 [17]. In addition, the parameter A is decided according to the assumption that Dreiding torsional potential should correspond to the dihedral torsional potential given in Eq. (4). It has been found that when A is equal to 10.02 kcal/mol, the Dreiding torsional potential is in a good agreement with the torsional potential. As a result, $m = 2$ and $A = 10.02$ kcal/mol were used in Eq. (5) for the Dreiding torsional potential.

For the non-bonded atomistic interaction, Lennard–Jones (L–J) potential

$$U_{\text{VDW}} = \left[\frac{A}{(r_{ij})^{12}} - \frac{B}{(r_{ij})^{6}}\right] \tag{6}$$

was employed to describe the van der Waals force between the carbon atoms where r_{ij} is the distance between the non-bonded pair of atoms. For the hexagonal graphite, the parameters $A = 1.171 \times 10^{-6}\,\frac{\text{kcal nm}^{12}}{\text{mol}}$ and $B = 6.675 \times 10^{-4}\,\frac{\text{kcal nm}^{6}}{\text{mol}}$ suggested in the literature [17] were adopted in the following simulation.

The atomistic structures of CNTs with minimized potential energy were constructed by performing NVT ensemble with time increment at 1 fs for 50 ps until the potential energy accomplished a stable value. Subsequently, the NPT ensemble with temperature at 0 K and pressure equal to 0 was conducted until the initial stress-free condition was accomplished.

2.2.2. Young's modulus E_1 in the longitudinal direction

In order to evaluate the properties of the equivalent solid cylinder, the potential energy of the CNTs in the initial state (stress-free state) was calculated through MD simulation. Subsequently, a small axial elongation was applied at one end of the CNTs with the other end being fixed. After an energy minimization process, the energy in the deformation configuration was evaluated again through the MD simulation. The simulation process is illustrated

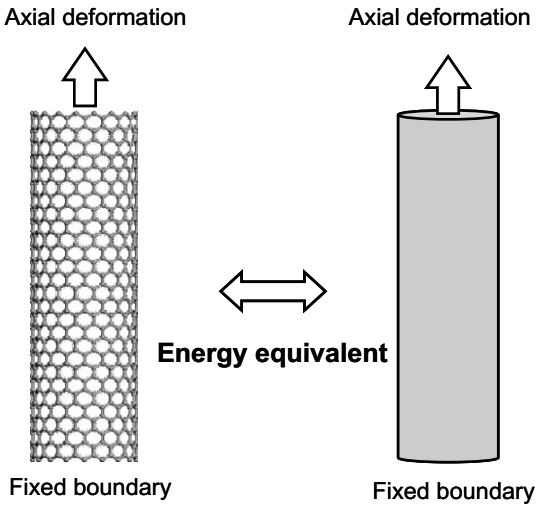

Fig. 4. Axial deformation applied in the CNT atomistic structures and the equivalent solid cylinder.

in Fig. 4. As a result, the potential energy variation between the initial and deformed configuration in CNT's atomistic structures associated with the axial strain increment was deduced.

On the other hand, when a continuum solid is subjected to simple tension, based on the linear elasticity theory, the Young's moduli can be derived from the strain energy variation with respective to the strain increment as

$$E_1 = \frac{2\Delta U}{\varepsilon^2 V_{\text{Solid}}} \tag{7}$$

where ΔU is the strain energy variation; ε is the strain increment; and V_{Solid} is the volume of the continuum solid. It is noted that the Poisson's effect was not considered in the above derivation. The potential energy variation obtained from the MD simulation was regarded as the energy difference in the equivalent solid associated with the same axial deformation. Through Eq. (7), the longitudinal moduli of the solid cylinder with three different radii were evaluated, and the results are presented in Table 1. It was observed that the Young's modulus of equivalent solid cylinder decreases as the cylinder radii increase. Basically, the trend matches with that presented in Ref. [11]. However, the Young's modulus of the equivalent solid cylinder is a little higher than those obtained in Ref. [11] for the same zig-zag type tubes. This discrepancy could be due to the different definitions of the cross-section area as well as the force potentials used in modeling the atomistic interaction of the carbon atoms. A critical review on the effective Young's moduli of carbon nanotubes has been presented in the literature [12,18].

2.2.3. Shear modulus G_{12} in the longitudinal direction

For the calculation of the shear modulus of the equivalent solid, the atomistic structure of CNTs was subjected to a torsional angle ϕ at one end together with the fixed boundary condition at the other end as shown in Fig. 5. Similar boundary was also adopted in the literature for the evaluation of the shear modulus of CNTs [19].

Table 1
Mechanical properties of equivalent solid cylinder.

Radius (Å)	3.9	5.5	7.1
E_1 (GPa)	1382.5	981.5	759.9
G_{12} (GPa)	1120	779.2	596.3
v_{12}	0.272	0.27	0.27
E_2 (GPa)	645	504	425
v_{23}	0.2	0.2	0.2

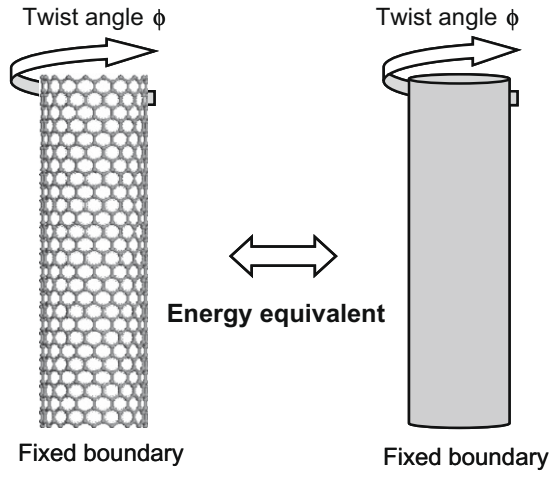

Fig. 5. Twist deformation applied on the CNT atomistic structure and the equivalent solid cylinder.

After the energy minimization process, the energy difference (ΔU) of the deformed CNTs with respect to the torsional angle ϕ was calculated through the MD simulation. If the deformation is very small and within the linear range, the associated shear modulus of the equivalent solid cylinder in terms of the torsional angle and energy variation is given as [20]

$$G_{12} = \frac{2\Delta U}{\phi^2 J_{\text{Solid}}} L_0 \tag{8}$$

where J_{Solid} is the cross-sectional polar inertia of the equivalent solid, and L_0 is the length of the CNTs. The shear moduli calculated with Eq. (8) for the equivalent solids are also shown in Table 1. Analogous to the longitudinal modulus, the shear modulus exhibits the declining behavior as the CNT radius increases.

2.2.4. Poisson's ratio v_{12}

In addition to the Young's modulus and shear modulus, the determination of Poisson's ratio of the equivalent solid was directly motivated by the continuum mechanics concept. Instead of the displacement constraints imposed on the boundaries, the axial stress was applied on the both ends of CNTs in order to diminish the end constraint effect. In the MD simulation, a modified NPT ensemble with the characteristics of varying simulation box in shape and size [21] was employed such that uniaxial stress can be independently applied at both ends of the CNTs with stress free in the lateral direction. Again after the energy minimization process, the equilibrated CNT atomistic structure was obtained, and then the Poisson's ratio was defined as

$$v_{12} = -\frac{\varepsilon_r}{\varepsilon} \tag{9}$$

where ε_r is the lateral strain in a nanotube and defined as $(r - r_0)/r_0$ in which r_0 and r are the CNT radius before and after the stress is applied, respectively. In addition, ε represents the axial strain. The Poisson's ratio obtained based on Eq. (9) for the zig-zag type CNTs with various radii are presented in Table 1. It seems that the Poisson's ratio of the equivalent solid cylinder is not sensitive to the CNT radius.

2.2.5. Young's modulus E_2 and Poisson's ration v_{23} in the lateral direction

Because of the characteristics of the atomistic structures of the CNTs, the mechanical properties in the lateral direction (in-plane properties) are isotropic; thus, only two material constants are independent and need to be determined. Here, Young's modulus E_2 and Poisson's ratio v_{23} in the transverse direction were selected in the following evaluation.

Radial displacement was applied on the atoms located at the circumference of the CNT atomistic structures as shown in Fig. 6, and then the energy variation of the CNTs after the deformation was calculated through the MD simulation. In a similar manner, the same amount of radial displacement was applied on the equiv-

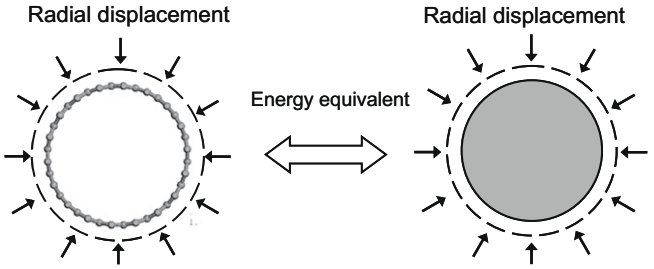

Fig. 6. Radial deformation applied on the CNT atomistic structure and the equivalent solid cylinder.

alent solid, and the energy variation was calculated through the finite element analysis. By adjusting the values of E_2 and v_{23} in the equivalent solid cylinder such that the energy variation in the equivalent solid is equal to that obtained from CNTs atomistic structure, the transverse properties in the effective solid were determined accordingly.

It is noted that in the equivalent solid, the energy variation is calculated using commercial finite element program ANSYS with a 2D plane element. Since only one equation (energy equivalence equation) is available, it is unfeasible to yield a unique solution for the two unknowns, E_2 and v_{23}, and thus multiple solutions are always generated in the above calculation. In order to understand the sensitivity of the E_2 and v_{23} values on the mechanical responses of CNT-reinforced nanocomposites, we assumed v_{23} as 0.2 and 0.4, respectively, and calculated the corresponding values of E_2 in the equivalent solids. Subsequently, the two different groups of E_2 and v_{23}together with other material constants, i.e., E_1, G_{12}, and v_{12}, were implemented into the Mori–Tanaka micromechanical model [22] for characterizing the properties of the CNT nanocomposites. Comparison of the moduli of the CNT nanocomposites obtained based on the two different properties of equivalent solids indicates that the mechanical properties of the CNTs composites are not dramatically affected by the transverse properties of the effective cylindrical solids. Therefore, we hereafter adopted v_{23} as 0.2 for the equivalent cylindrical solid and then calculated the related Young's modulus E_2. All mechanical properties of equivalent cylindrical solid calculated based on the energy equivalence concept are summarized in Table 1.

3. Effective interphase model

When the hollow molecular structure of a CNT was converted into a solid cylinder through the energy equivalent concept as presented in the early section, the mechanical behavior of CNT nanocomposites can be predicted using the conventional two-phase micromechanical model [22]. In the two-phase model, it is always assumed that the reinforcements are perfectly bounded with the surrounding polymeric matrix. However, in CNT-reinforced nanocomposites, the interfacial bonding is not perfect, but it is dominated by the non-bonded interaction that consists of the electrostatic and van der Waals interactions. Moreover, the extent of atomistic interaction between the CNTs and surrounding matrix may have an influence on the mechanical responses of the nanocomposites. As a result, it is indispensable to have a continuum micromechanical model being able to account for the inter-atomic effect in the modeling of CNTs nanocomposites. In this section, the atomistic interaction between the CNTs and the polyimide matrix was characterized through the effective interphase, the corresponding properties of which were determined from the molecular interaction energy calculated from MD simulation. With the properties of the effective interphase in conjunction with the equivalent solid cylinder of CNTs, the CNT nanocomposites that originally are discrete atomistic structures can be interpreted by using a three-phase continuum micromechanical model as demonstrated in Fig. 7.

3.1. Construction of CNTs/polyimide molecular structures

In order to understand the atomistic interaction between the CNTs and the surrounding polyimide polymer, the molecular structure of CNTs/polyimide nanocomposites employed in the MD simulation were constructed initially. A simulation unit with periodic boundary conditions that contain a CNT embedded in the amorphous polyimide molecular chains is constructed as shown in Fig. 7(a). The polyimide polymer is generated by 10 repeated monomer units, and the corresponding chain number is dependent on the size of the simulation box. Fig. 8 illustrates the polyimide monomer unit. It is noted that the Dreiding force field [17] was employed to describe the covalent bonding as well as the non-

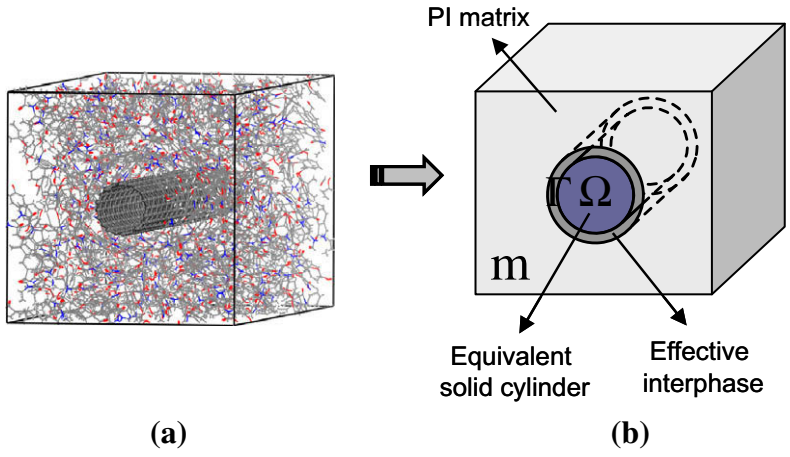

Fig. 7. Schematic representation of simulation process: (a) CNTs/polyimide molecular structure and (b) three-phase micromechanical model.

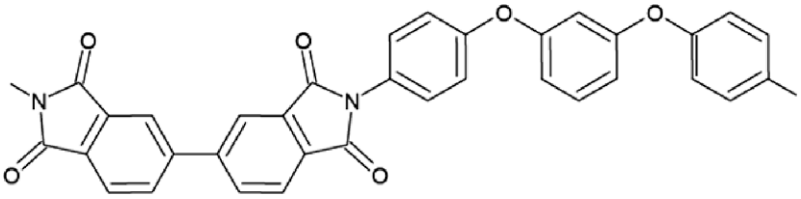

Fig. 8. Sketch of polyimide monomer unit.

bonding interaction in the polyimide polymer. In addition, the atomistic interaction between polyimide molecular and CNTs were also directly modeled using the Dreiding force field although the modified parameters in Dreiding force field were employed to model the CNTs as discussed earlier. Three different sizes of CNTs, 3.9, 5.5, and 7.1 Å in radius, were considered individually as reinforcements in the nanocomposites, and the corresponding numbers of polyimide chains equal to 8, 16, and 26, respectively, were utilized in these CNT/polyimide molecular structures in order that the volume fractions of CNTs in the nanocomposites remain the same.

The MD simulations for the CNT/polyimide nanocomposites were conducted using a DL-POLY package [16]. The equilibrated molecular structure with minimized energy was accomplished by sequentially performing the NVT and NPT ensembles in the MD simulation. It is noted that NVT ensemble stands for the volume and temperature being fixed during the simulation, and NPT ensemble represents that the pressure and temperature remain constant during the simulation. The purpose of the NVT ensemble conducted at 1000 K for 200 ps was to supply enough kinetic energy on the polyimide molecular so that homogeneous molecular structure within the simulation box can be achieved. During the process, the CNT atoms were *frozen*, which designates that the carbon atoms on CNTs were fixed at their original position throughout the whole simulation [23]. Subsequently, the NPT process was designated to 0 atm such that the simulation box with traction-free boundary conditions could be satisfied. Two sub-steps were introduced for the temperature drop from 1000 to 0 K in the NPT process. In the first step, the temperature was designated at 300 K for 200 ps, and in the second stage, the frozen atoms in the CNT structures were released, and the entire system was equilibrated at 0 K under stress-free conditions for another 100 ps. During the simulation, the total potential energy variation was examined, and when the quantity fluctuated around a certain mean value for a while, the system was considered to be in equilibrium. Figs. 9 and 10 demonstrate the potential energy history of the nanocomposites as well as the temperature variation during the second step in the NPT ensemble, respectively. It seems that the potential energy attains stable condition after 10 ps, and meanwhile, the temperature is approaching 0 K. Based on the observations, it was suggested that the current molecular structure is in the equilibrium condition and suitable for the characterization of the molecular structures as well as the material properties.

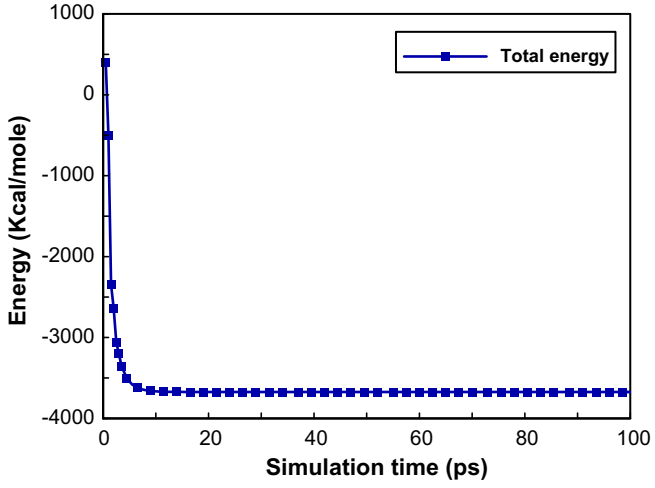

Fig. 9. Variation of potential energy in NPT ensemble.

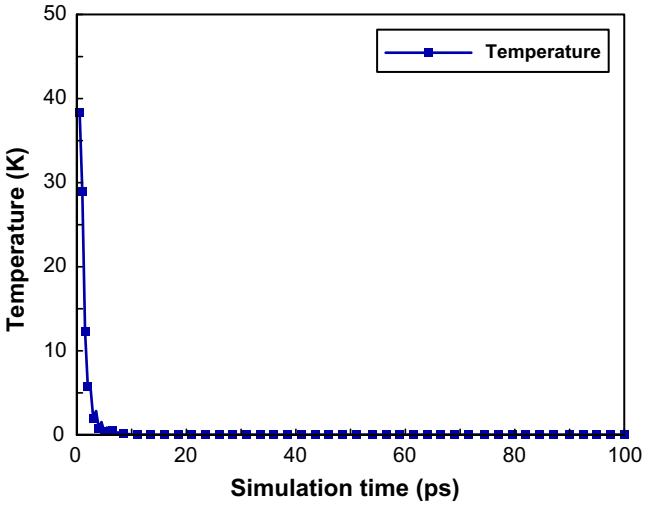

Fig. 10. Variation of temperature in NPT ensemble.

3.2. Non-bonded gap

The density distribution of polyimide polymer near the CNTs was initially examined according to the following formulation

$$\rho(r) = \frac{g_r}{V_r} \tag{10}$$

where $V_r = \pi((r+dr)^2 - r^2)L_0$ indicates the volume of a cylindrical shell near the CNTs with length equal to L_0 as shown in Fig. 11, and g_r denotes the total atom mass in V_r. The density distribution of the CNTs and the PI polymer in the radial direction is illustrated in Fig. 12. It can be seen that near the CNTs, the polyimide density is relatively high and then declines to a typical value $(1.31\,g/cc)$ [24] when it is far away from the CNTs. In addition, there is a clear gap with very low molecular density existing between the CNTs and the surrounding polyimide matrix. In this study, the gap has been referred to as the non-bonded gap because it is caused by the non-bonded force field between the CNTs and the polymeric matrix. In order to qualitatively characterize the dimension of the non-bonded gap, a radial volume element, as shown in Fig. 13, is proposed, where $\Delta\theta$ is the angle between two radial lines emitted from the center of the CNTs, and Δz is the length in the CNTs longitudinal

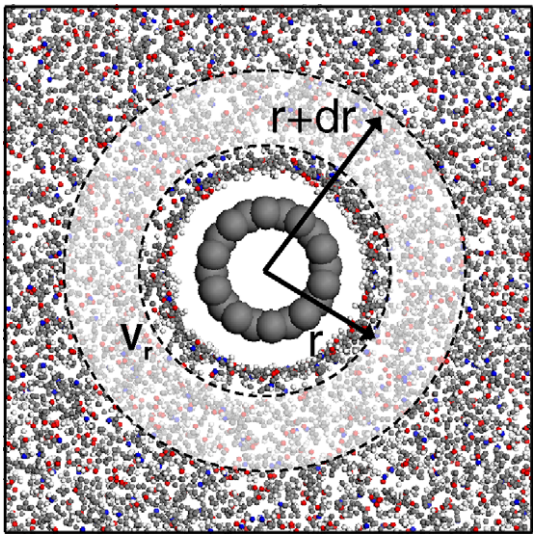

Fig. 11. Evaluation of density distribution of polyimide polymer in the radial direction.

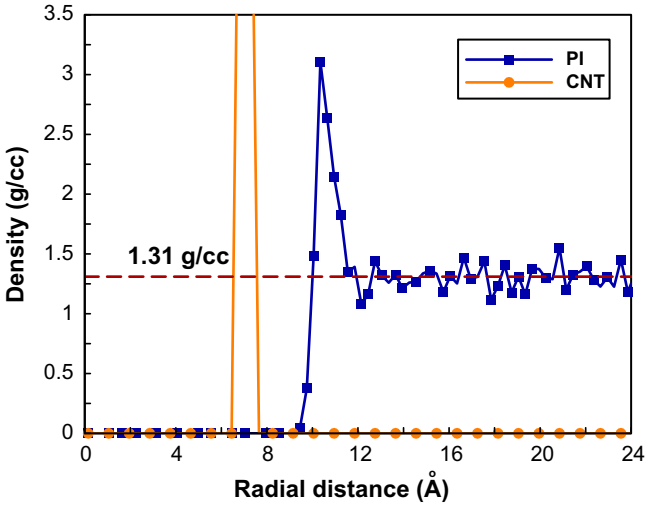

Fig. 12. Density distributions of the CNTs and polyimide in the radial direction.

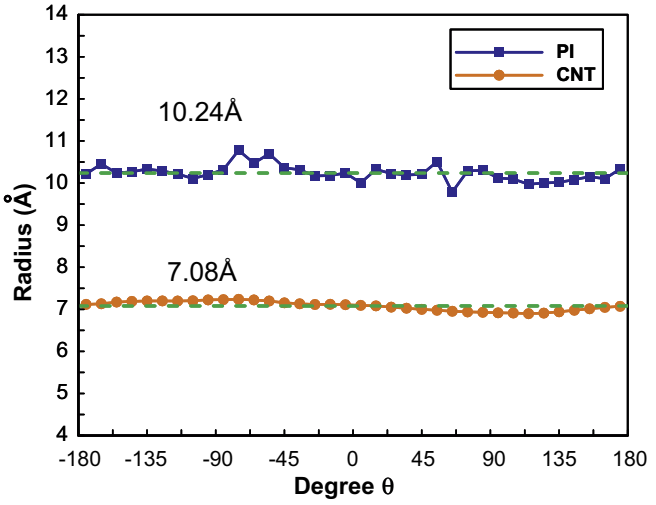

Fig. 14. Measurements of the maximum radial distance for CNTs atoms and the minimum radial distance for polyimide atoms within the radial volume element.

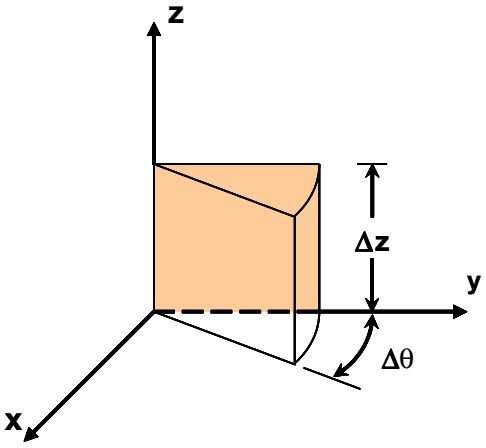

Fig. 13. Schematic of the radial volume element for the non-bonded gap ($\Delta\theta = 10^\circ, \Delta z = 10$ Å).

direction. For each incremental rotation (10°) of the volume element with respective to the *z*-axis, the positions of the CNTs and polyimide atoms within the element were counted. The maximum radial distance for the CNTs atoms within the volume element is denoted as $r_{\text{CNTs}}^{\max}$, and the minimum radial distance for the polyimide atoms is represented as $r_{\text{PI}}^{\min}$. The non-bonded gap between the CNTs and the polyimide matrix within the unit volume is introduced as

$$r_{\text{non-bonded}} = r_{\text{PI}}^{\min} - r_{\text{CNTs}}^{\max} \tag{11}$$

Fig. 14 illustrates the measurements of the maximum radial distance for CNTs atoms together with the minimum radial distance for polyimide atoms for each rotational increment. When the radial volume element rotates around 360°, the average value of the $r_{\text{non-bonded}}$ is regarded as the non-bonded gap of the nanocomposites. Table 2 indicates the non-bonded gap calculated from the nanocomposites with three different CNT radii. It seems that the non-bonded gap decreases a little bit as the CNT radius increases. Nevertheless, the dependence of the non-bonded gap on the CNT radius was found to be not so significant.

3.3. Non-bonded energy

In addition to the non-bonded gap, the non-bonded energy between the CNTs and the polyimide matrix was also estimated from the MD simulation. In the calculation of the non-bonded interaction, only the van der Waals interaction that was modeled by Lennard–Jones potential function was considered. It should be noted that, in reality, some kind of cross-linking between the CNTs and polyimide matrix may be constructed in the curing process. This phenomenon has not been included in the present modeling. The total non-bonded energy within the nanocomposites is contributed not only by the interaction between the CNTs and the polyimide, but also by the CNTs as well as the polyimide molecular chains. Therefore, the non-bonded energy between the CNTs and polyimide is calculated by subtracting the non-bonded energy of the CNTs and polyimide polymer from the total non-bonded energy, and it can be expressed as

Table 2
Non-bonded gap and normalized non-bonded energy in CNT/polyimide nanocomposites with various CNTs radii.

Radius (Å)	3.9	5.5	7.1
Non-bond gap (Å)	3.333	3.236	3.158
Normalized non-bond energy (J/m^2)	0.3560	0.3269	0.3142

$$U_{\text{PI-CNTs}} = U_{\text{total}} - U_{\text{CNTs}} - U_{\text{PI}} \tag{12}$$

where U_{total} is the total non-bonded energy obtained from the nanocomposites. U_{CNTs} and U_{PI} stand for the non-bonded energy of CNTs and polyimide molecular chain, respectively. The non-bonded energy of the polyimide molecular chain was evaluated in the simulation box where the CNTs were removed, and only the molecular structures of the polyimide matrix were left. In a similar manner, the non-bonded energy of CNTs was calculated. Therefore, with Eq. (12), the non-bonded energy between the CNTs and the polyimide was determined. It is worthy to note that the non-bonded energy provides a relative indication regarding the extent of interaction between the CNTs and the surrounding matrix. If the non-bond interaction can be further employed to represent the properties of an equivalent interphase with the dimension equal to the non-bond gap, it is possible that the mechanical properties of the nanocomposites could be described by the three-phase micromechanical model comprising the CNTs, effective interphase, and polyimide polymer.

To achieve this goal, the degree of interaction between the CNTs and the matrix is characterized in terms of the normalized non-bonded energy, which is defined as the non-bonded energy divided

by the surface area of the CNTs. Subsequently, the normalized non-bonded energy was assumed to be associated with the non-bonded gap in the form as

$$U(r) = \frac{1}{6}kr^6 \tag{13}$$

where r is the non-bonded gap, and k is the parameter to be determined. Based on the normalized non-bonded energy, the corresponding normalized interaction force was obtained by differentiating the energy with respect to the distance as

$$F(r) = -\frac{\partial U}{\partial r} = -kr^5 \tag{14}$$

The negative sign of the force in Eq. (14) represents the attractive interaction. On the other hand, Eqs. (13) and (14) can also be interpreted as the strain energy of a unit element with length equal to the non-bond gap, r, and the cross-section area equal to 1, when it is subjected to the applied loading kr^5. Therefore, from the 1D elasticity, the strain energy of the unit element is represented as

$$U = \frac{\sigma^2}{2E}r \tag{15}$$

where E is the Young's modulus of the equivalent unit element, and σ is equal to kr^5 that is the loading applied on the unit area (so-called stress). From the hypothesis that the strain energy of the unit element is equivalent to the normalized energy given in Eq. (13), the modulus of the equivalent unit element is yielded as

$$E = 3kr^5 = \frac{18U(r)}{r} \tag{16}$$

It is noted that in the above calculation, only the strain energy caused by axial loading was adopted to illustrate the normalized non-bonded energy of the nanocomposites obtained from the MD simulation. As a result, once the non-bonded gap as well as the normalized non-bonded energy was calculated, the elastic moduli of the equivalent interphase can be determined by means of Eq. (16). Table 2 demonstrates the normalized non-bonded energy of the nanocomposites calculated with different CNTs radii. It shows that as the radius increases, the corresponding normalized non-bonded energy decreases, which indicates the interaction is lessening.

3.4. Three-phase micromechanical model

Based on the aforementioned derivation, the non-bonded interaction between the CNTs and the surrounding polyimide matrix can be appropriately replicated by a continuum-based equivalent interphase. With the mechanical properties of the equivalent solid cylinder (representing CNTs), effective interphase, and polyimide matrix as well as the corresponding geometric parameters, the responses of the CNTs nanocomposites can be depicted using the micromechanical model with multiple phases [25,26]. It should be noted that three ingredients have been considered in the three-phase model, which is different from conventional Mori–Tanaka micromechanical model [22] where only two phases are included in the analysis. The explicit formulation of the three-phase model is written as [25]

$$C^* = C^m + \left[(v_\Gamma + v_\Omega)\{C^\Gamma - C^m\}A_V^{\mathrm{di}} + v_\Omega\left\{(C^\Omega - C^\Gamma)A_\Omega^{\mathrm{di}}\right\}\right]\left[v_m I + (v_\Gamma + v_\Omega)\left\{A_V^{\mathrm{di}}\right\}\right]^{-1} \tag{17}$$

where C^* denotes the stiffness matrix for the nanocomposites, C^Ω, C^Γ, and C^m represent the stiffness of the domain of Ω (equivalent solid), Γ (interphase), and m (polyimide matrix), respectively, as shown in Fig. 7(b); v_Ω, v_Γ, and v_m indicate the volume fraction of the respective domains. In addition,

$$A_V^{\mathrm{di}} = I + E_{\mathrm{Esh}}^V \Phi^V \tag{18}$$

$$A_\Omega^{\mathrm{di}} = I + \Delta E_{\mathrm{Esh}}\Phi^\Gamma + E_{\mathrm{Esh}}^\Omega \Phi^\Omega \tag{19}$$

where

$$\Phi^\Omega = -\left[\left(E_{\mathrm{Esh}}^\Omega + C^1\right) + \Delta E_{\mathrm{Esh}}\left(E_{\mathrm{Esh}}^\Omega - \frac{v_\Omega}{v_\Gamma}\Delta E_{\mathrm{Esh}} + C^2\right)^{-1}\left(E_{\mathrm{Esh}}^\Omega - \frac{v_\Omega}{v_\Gamma}\Delta E_{\mathrm{Esh}} + C^1\right)\right]^{-1} \tag{20}$$

$$\Phi^V = \frac{v_\Omega}{v_\Omega + v_\Gamma}\Phi^\Omega + \frac{v_\Gamma}{v_\Omega + v_\Gamma}\Phi^\Gamma \tag{21}$$

$$\Phi^\Gamma = -\left[\Delta E_{\mathrm{Esh}} + \left(E_{\mathrm{Esh}}^\Omega + C^1\right)\left(E_{\mathrm{Esh}}^\Omega - \frac{v_\Omega}{v_\Gamma}\Delta E_{\mathrm{Esh}} + C^1\right)^{-1}\left(E_{\mathrm{Esh}}^\Omega - \frac{v_\Omega}{v_\Gamma}\Delta E_{\mathrm{Esh}} + C^2\right)\right]^{-1} \tag{22}$$

$$\Delta E_{\mathrm{Esh}} = E_{\mathrm{Esh}}^\Omega - E_{\mathrm{Esh}}^V \tag{23}$$

$$C^1 = (C^\Omega - C^m)^{-1}C^m \tag{24}$$

$$C^2 = (C^\Gamma - C^m)^{-1}C^m \tag{25}$$

In the above expression, $V = \Omega + \Gamma$, which is the domain comprising the CNTs and the interphase as well, and E_{Esh}^V and E_{Esh}^Ω indicate the Eshelby's tensor for the domains V and Ω, respectively [27]. It is noted that when the aspect ratio of the inclusion phases are infinite, such as CNTs, the Eshelby's tensors can be written explicitly as [28]

$$E_{\mathrm{Esh}}^\Omega = E_{\mathrm{Esh}}^V = E_{ijkl} \tag{26}$$

where

$$E_{1111} = 0 \tag{27}$$

$$E_{2222} = E_{3333} = \frac{5 - 4v_m}{8(1 - v_m)} \tag{28}$$

$$E_{2233} = E_{3322} = \frac{4v_m - 1}{8(1 - v_m)} \tag{29}$$

$$E_{2211} = E_{3311} = \frac{v_m}{2(1 - v_m)} \tag{30}$$

$$E_{1122} = E_{1133} = 0 \tag{31}$$

$$E_{2323} = \frac{3 - 4v_m}{8(1 - v_m)} \tag{32}$$

$$E_{1212} = E_{1313} = \frac{1}{4} \tag{33}$$

and v_m is the Poisson's ratio of the surrounding matrix. In the above approach, the discrete molecular structure of CNT nanocomposites was efficiently converted into a continuum system, and the corresponding properties could be simulated using the continuum micromechanical analysis when the equivalent properties were properly determined.

4. Elastic constants of molecular structures

In addition to the micromechanical analysis previously discussed, the mechanical properties of the equilibrated molecular configuration of CNTs nanocomposites were also predicted using the molecular dynamic simulation. A modified NPT ensemble with the characteristics of varying simulation box in shape and size [21] was subjected to uniaxial tension. After the energy minimization process, the deformed configuration of the nanocomposites was obtained from which the strain increment in the loading direction was calculated, and the associated stress was then calculated from the virial theorem [29]. It is noted that on the lateral surfaces of the simulation box, stress-free condition was imposed in order to simulate the simple tension condition [30]. Therefore, the modulus of the nanocomposites in the loading direction can be measured as the ratio of the stress associated with the corresponding strain increment

$$E = \frac{\Delta\sigma}{\Delta\varepsilon} \tag{34}$$

In this study, the moduli of the CNTs nanocomposites in the longitudinal and transverse directions were estimated, respectively, from the molecular dynamic simulation, and the results were compared with those derived from the three-phase micromechanical model.

5. Results and discussions

Table 3 shows the longitudinal moduli of the CNTs/polyimide nanocomposites with three different radii of CNTs. It seems that as the radius increases, the corresponding modulus of the nanocomposites decreases although the CNTs volume fractions remain the same. In addition, the moduli of the nanocomposites calculated from the MD simulation are quite close to the conventional micromechanical model (rule of mixture). Thus, the effect of atomistic interaction between the CNTs and polyimide may be neglected in modeling the longitudinal modulus of nanocomposites with continuous CNTs as indicated in Refs. [4,5]. Because of the influence of the effective interphase, the longitudinal modulus of the nanocomposites obtained from the three-phase model is little higher than that obtained from the MD simulation.

On the other hand, for the transverse moduli of the CNT/polyimide nanocomposites, the results with different radii of CNTs are listed in Table 4. Similar to the longitudinal moduli, the transverse moduli is also decreasing when the CNTs radii increase. Nonetheless, the declining characteristic observed in the MD simulation and three-phase model was not exhibited in the conventional micromechanical model. Apparently, in the transverse direction, the atomistic interaction effect is more significant, but not accounted for, in the conventional continuum mechanics modeling. In the light of the forgoing discussion, it is suggested that in the longitudinal direction, the conventional micromechanical model with the equivalent CNT properties is adequate for predicting the moduli of CNT nanocomposites. Alternatively, for the transverse modulus of the nanocomposites, the three-phase model has to be employed in the description of the mechanical properties with accuracy. In addition, for the reinforcement efficiency, it has been revealed that the CNTs with smaller radii can provide better mechanical properties in their composites when the volume fractions of CNTs remain the same. This suggestion is consistent with the experimental observations that the efficiency of reinforcement varies linearly with the total CNT's surface area in the nanocomposites [31].

Table 3
Comparison of longitudinal Young's moduli of CNT/polyimide nanocomposites obtained from MD simulation, Mori–Tanaka model and three-phase model.

Radius (Å)	3.9	5.5	7.1
Volume fraction of CNT (%)	6.28	6.43	6.67
Young's modulus (GPa) (MD simulation)	90.6	67.6	54.2
Young's modulus (GPa) (Mori–Tanaka model)	90.6	66.9	54.7
Young's modulus (GPa) (three-phase model)	92.9	68.3	55.8

Table 4
Comparison of transverse Young's moduli of CNT/polyimide nanocomposites obtained from MD simulation, Mori–Tanaka model and three-phase model.

Radius (Å)	3.9	5.5	7.1
Volume fraction of CNT (%)	6.28	6.43	6.67
Transverse Young's modulus (GPa) (MD simulation)	6.22	5.86	5.29
Transverse Young's modulus (GPa) (Mori–Tanaka model)	5.28	5.27	5.28
Transverse Young's modulus (GPa) (three-phase model)	6.32	5.90	5.74

6. Conclusion

The mechanical properties of the CNT/polyimide nanocomposites were characterized using multi-scale simulation. The equivalent cylindrical solid was proposed to model the atomistic structure of CNTs, and the corresponding properties were determined from the molecular mechanics in conjunction with the energy equivalence concept. The level of atomistic interaction between the CNTs and the surrounding polyimide polymer was modeled by the effective interphase, the properties of which were obtained from the non-bonded energy as well as the non-bonded gap determined from the MD simulation. With the properties of equivalent solid cylinder, effective interphase, and polyimide polymer, the mechanical properties of CNTs nanocomposites can be predicted using the three-phase continuum micromechanical model. For comparison purposes, the two-phase micromechanical model (Mori–Tanaka model) was also adopted in the prediction. A comparison of the micromechanical results with the MD results indicates that the longitudinal moduli of the CNT nanocomposites can be precisely predicted using the two-phase micromechanical model together with the equivalent cylinder properties of the CNTs. However, in the transverse direction, the three-phase model can provide better results than the two-phase micromechanical model since the atomistic interactions between the CNTs and polyimide polymer become essential in such conditions.

References

[1] Lau KT, Gu C, Hui D. A critical review on nanotube and nanotube/nanoclay related polymer composite materials. Composites B 2006;37(6):425–36.
[2] Thostenson ET, Li C, Chou TW. Nanocomposites in context. Compos Sci Technol 2005;65(3–4):491–516.
[3] Han Y, Elliott J. Molecular dynamics simulations of the elastic properties of polymer/carbon nanotube composites. Comput Mater Sci 2007;39(2):315–23.
[4] Griebel M, Hamaekers J. Molecular dynamics simulations of the elastic moduli of polymer–carbon nanotube composites. Comput Methods Appl Mech Eng 2004;193(17–20):1773–88.
[5] Zhu R, Pan E, Roy AK. Molecular dynamics study of the stress–strain behavior of carbon-nanotube reinforced Epon 862 composites. Mater Sci Eng A 2007;447(1–2):51–7.
[6] Liu YJ, Chen XL. Evaluations of the effective material properties of carbon nanotube-based composites using a nanoscale representative volume element. Mech Mater 2003;35(14):69–81.
[7] Luo D, Wang WX, Takao Y. Effects of the distribution and geometry of carbon nanotubes on the macroscopic stiffness and microscopic stresses of nanocomposites. Compos Sci Technol 2007;67(14):2947–58.
[8] Selmi A, Friebel C, Doghri I, Hassis H. Prediction of the elastic properties of single walled carbon nanotube reinforced polymers: a comparative study of several micromechanical models. Compos Sci Technol 2007;67(10):2071–84.
[9] Hammerand DC, Seidel GD, Lagoudas DC. Computational micromechanics of clustering and interphase effects in carbon nanotube composites. Mech Adv Mater Struct 2004;14(4):277–94.
[10] Gates TS, Odegard GM, Frankland SJV, Clancy TC. Computational materials: multi-scale modeling and simulation of nanostructured materials. Compos Sci Technol 2005;65(15-16):2416–34.
[11] Suzuki K, Nomura S. On elastic properties of single-walled carbon nanotubes as composite reinforcing fillers. J Compos Mater 2007;41(9):1123–35.
[12] Lau KT, Chipara M, Ling HY, Hui D. On the effective elastic moduli of carbon nanotubes for nanocomposite structures. Composites B 2004;35(2):95–101.
[13] Rappe AK, Casewit CJ. Molecular mechanics across chemistry. Sausalito, CA: University Science Books; 1997.
[14] Li C, Chou TW. A structural mechanics approach for the analysis of carbon nanotubes. Int J Solids Struct 2003;40(10):2487–99.
[15] Cornell WD, Cieplak P, Bayly CI, Gould IR, Merz Jr KM, Ferguson DM, et al. A second generation force field for the simulation of proteins, nucleic acids, and organic molecules. J Am Chem Soc 1995;117(19):5179–97.
[16] Smith W, Forester TR. DLPOLY-2.13 manual; 2001.
[17] Mayo SL, Olafson BD, Goddard III WA. Dreiding: a generic force field for molecular simulations. J Phys Chem 1990;94(26):8897–909.
[18] Tserpes KI, Papanikos P. Finite element modeling of single-walled carbon nanotubes. Composites B 2005;36(5):468–77.
[19] Wang Y, Wang XX, Ni X. Atomistic simulation of the torsion deformation of carbon nanotubes. Modell Simul Mater Sci Eng 2004;12(6):1099–107.
[20] Gere JM. Mechanics of materials. Cheltenham, UK: Nelson Thornes; 2001.
[21] Melchionna S, Ciccotti G, Holian BL. Hoover NPT dynamics for systems varying in shape and size. Mol Phys 1993;78(3):533–44.
[22] Mori T, Tanaka K. Average stress in matrix and average elastic energy of materials with misfitting inclusions. Acta Metall 1973;21(5):571–4.

[23] Adnan A, Sun CT, Mahfuz H. A molecular dynamics simulation study to investigate the effect of filler size on elastic properties of polymer nanocomposites. Compos Sci Technol 2007;67(3–4):348–56.
[24] Ashby MF, Jones DR. Engineering materials 1: an introduction to their properties and applications. Oxford: Butterworth; 1996.
[25] Dunn ML, Ledbetter H. Elastic moduli of composites reinforced by multiphase particles. J Appl Mech 1995;62(4):1023–8.
[26] Hori M, Nemat-Nasser S. Double-inclusion model and overall moduli of multi-phase composites. Mech Mater 1993;14(3):189–206.
[27] Eshelby JD. The determination of the elastic field of an ellipsoidal inclusion, and related problems. Proc R Soc Lond Ser A 1957;241(1226):376–96.
[28] Qiu YP, Weng GJ. On the application of Mori–Tanaka's theory involving transversely isotropic spheroidal inclusions. Int J Eng Sci 1990;28(11):1121–37.
[29] Allen MP, Tildesley DJ. Computer simulation of liquids. Oxford: Clarendon Press; 1987.
[30] Cho J, Sun CT. A molecular dynamics simulation study of inclusion size effect on polymeric nanocomposites. Comput Mater Sci 2007;41(1): 54–62.
[31] Cadek M, Coleman JN, Ryan KP, Nicolosi V, Bister G, Fonseca A, et al. Reinforcement of polymers with carbon nanotubes: the role of nanotube surface area. Nano Lett 2002;4(2):353–6.